The nuclear spectrum of the radio galaxy NGC 5128 (Centaurus A)

Chris Simpson[1] and Vikki Meadows
Jet Propulsion Laboratory, California Institute of Technology, 4800 Oak Grove Drive, Pasadena, CA 91109

ABSTRACT

We present near-infrared spectra of the nucleus of the nearby radio galaxy NGC 5128 (Centaurus A). The observed emission line strengths suggest that NGC 5128 should be classified as a LINER, and appear to be powered by shocks. This conclusion is supported by a number of similarities between NGC 5128 and M 87, whose ultraviolet emission line spectrum unequivocally supports shock excitation. We deduce that the central black hole mass in NGC 5128 is probably no more than $10^9\,M_\odot$.

Subject headings: galaxies: active — galaxies: individual (NGC 5128, Centaurus A) — galaxies: nuclei — infrared: galaxies

1. Introduction

The galaxy NGC 5128 hosts the extragalactic radio source Centaurus A. It is our nearest radio galaxy, and has been the subject of intense study. These studies have revealed a jet which is seen at radio, near-infrared, and X-ray wavelengths (Meier et al. 1989; Joy et al. 1991; Schreier et al. 1979), and an unresolved nucleus which appears at wavelengths beyond $2\,\mu$m (Turner et al. 1992). Perhaps the most obvious feature of NGC 5128, however, is the dust lane which straddles the galaxy. Such prominent and well-ordered dust obscuration is more commonly associated with spirals, and is unusual for an early-type galaxy (although perhaps not for a radio galaxy: Osterbrock 1983; de Koff et al. 1996). It is widely believed that the dust lane was formed from material stripped from a dusty disk galaxy (Baade & Minkowski 1954; Thomson 1992). A natural consequence of this merger would be substantial star formation, and there is extended emission within the dust lane

[1]Present address: Subaru Telescope, 650 N. A'Ohōkū Pl., Hilo, HI 96720

that Quillen, Graham & Frogel (1993) attributed to small dust grains which are heated by ultraviolet photons from young stars. Meadows & Allen (1992) rejected dust as the source of the emission and instead proposed that the emission comes from red giants and/or supergiants. While not supportive of an extended starburst, Meadows & Allen did suggest that there might be a compact region of star formation at the nucleus, on the basis of a near-infrared spectrum covering the H and K spectroscopic windows.

A spectroscopic study of the nucleus of NGC 5128 presents a number of problems. Extinction from the dust lane affects the observed emission line ratios, especially in the optical part of the spectrum. More basic than that, however, is the difficulty in actually locating the nucleus. The position of the continuum peak varies with wavelength as a result of patchy extinction in the dust lane, and the true nucleus only reveals itself at wavelengths longer than $2\,\mu$m when the unresolved emission from the active nucleus is seen (Turner et al. 1992). Due in part to the small field of view of current infrared imagers, accurate astrometry has so far not been possible and the nucleus can only be acquired by locating the peak of the K-band emission prior to taking a spectrum. The InfraRed Imaging Spectrometer on the 3.9-m Anglo-Australian Telescope, IRIS (Allen et al. 1993), has the capability to image a field before inserting the dispersing element, and we have used it to obtain spectra of the nucleus covering the wavelength range $0.9\,\mu\mathrm{m} < \lambda < 2.5\,\mu\mathrm{m}$. We present these spectra in this paper, and use them to investigate the excitation mechanism operating at the nucleus of NGC 5128.

Throughout this paper, we adopt a distance of 3.6 Mpc to NGC 5128 (Soria et al. 1996), producing a projected linear scale of $17\,\mathrm{pc\,arcsec^{-1}}$.

2. Observations and reduction

For this work, data were taken with both narrow (1.″4) and wide (5.″8) slits at a spatial resolution of $0.''8\,\mathrm{pixel^{-1}}$. IRIS was configured to use the IJ (0.9–1.5 μm) and HK (1.4–2.5 μm) echelles and provided a spectral resolution of $\lambda/\Delta\lambda \sim 400$ (narrow slit) or ~ 100 (wide slit). All spectra were taken with the slit oriented east–west. The true nucleus of NGC 5128 was acquired by locating the continuum peak at K', and spectra were taken at either end of the 13″ slit and differenced to remove the sky and underlying galaxy. All data were taken in approximately 2″ seeing. Narrow slit HK echelle data were taken on the nights of UT 1991 April 26/27 and 1991 June 25/26 for a total integration time of 7400 s, and have already been presented in Meadows & Allen (1992). Narrow slit IJ data totaling 2000 s were taken on UT 1992 April 14. Wide slit data were taken on UT 1992 September 13, with an exposure time of 1200 s in each of the two echelles.

The data were reduced using standard spectral reduction techniques to remove the spatial and spectral response of the detector, the curvature of the echelle orders, and the apparent rotation of the slit, which changes across the orders. One-dimensional spectra were extracted from the echelle orders using a either two or three-pixel (1.″6 or 2.″4) extraction apertures. The narrow slit spectra, which were taken in non-photometric conditions, have been flux calibrated by scaling the continuum fluxes so that they matched photometry from the images of Meadows & Allen (1992), which in turn were calibrated using the aperture photometry of Turner et al. (1992). We estimate that the systematic uncertainties introduced by this method are less than 20%; the ratios derived from line pairs within the IJ or HK echelles are, of course, unaffected. Observations of standard stars were used to calibrate the wide slit data which in turn was used as a calibration cross-check for the narrow slit data.

3. Results and analysis

The narrow slit spectrum is shown in Figure 1. We present the extracted line fluxes in Table 1. These fluxes were obtained by measuring the signal above a linear continuum level which was determined by eye. It is the placement of this continuum which is the dominant source of uncertainty in the measurements, and so the uncertainty was determined by making several measurements with different 'reasonable' continuum levels. Not surprisingly, the measurement uncertainties from the narrow slit data are much smaller than those from the wide slit spectra, due to the lower sky noise. In particular, Paγ, and [Fe II] $\lambda 1.6435\,\mu$m are strongly affected by poor sky subtraction in the wide slit data, which manifests itself as a substantial broadening of the emission line. He I $\lambda 1.0830\,\mu$m is also affected because it is blended with Paγ in the low resolution wide slit data.

3.1. Reddening to the emission line region

Both of the near-infrared [Fe II] lines are produced by radiative de-excitation from the $^4D_{7/2}$ level of Fe^+, and so their intensity ratio is fixed at 0.74 (Nussbaumber & Storey 1988), with the shorter wavelength line being the stronger of the two. Their observed ratio can therefore be used as a reddening indicator, and the narrow slit data suggest $A_V = 3\,\mathrm{mag}$[2], although they are also consistent with zero reddening, and provide a formal 3σ upper limit

[2]We use the parameterized extinction law of Cardelli, Clayton & Mathis (1989) with $R_V = 3.1$, although other laws produce nearly identical results.

of $A_V < 8$ (this upper limit includes the relative photometric uncertainty between the *IJ* and *HK* echelle data). The 1.6435 μm line is strongly affected by poor sky subtraction in the wide slit data, and therefore no useful ratio can be obtained.

The only reliable H I line ratio we have from the wide slit data is Paβ/Brγ = 1.25±0.25. Compared to the Case B ratio of 5.88, this implies an extinction of $A_V = 10.9 \pm 2.2$ to the emission line region. Although the Paβ/Brγ and Paγ/Brγ ratios from the narrow slit data are less reliable due to the method of flux calibration, they too support a value for the extinction of about ten magnitudes. However, the observed narrow slit Paβ/Paγ = 1.83 ± 0.35 is consistent with the Case B value of 1.81, implying negligible reddening, whereas if $A_V \approx 10$, it should be twice as large. A formal 3σ upper limit to the extinction based on this ratio (which is not affected by flux calibration uncertainties) is $A_V < 7.7$ mag. We therefore conclude that the Brγ flux is increased by an additional component which, presumably by virtue of being heavily reddened, does not contribute to the flux of the observed Paschen lines. This could plausibly be a contribution from a putative broad line region. If the broad line region suffers the $A_V \sim 30$ mag of extinction which obscures the nuclear continuum (Giles 1986; Meadows & Allen 1992) then the broad Brγ flux will be reduced by a factor of about 20. If the broad line is intrinsically 40 times more luminous than the narrow line (e.g. Jackson & Eracleous 1995), then the ratio of narrow Paβ/Br$\gamma \approx 4$, corresponding to $A_V \approx 3$, in line with that derived from the [Fe II] ratio. An extinction of $A_V \approx 3$ mag is also consistent with obscuration from the dust lane alone, based on the observed nuclear $J - H$ color if we assume that approximately half the nuclear *H* band emission is non-stellar (Meadows & Allen 1992), and we adopt this value for the extinction to the emission line region.

3.2. Morphology of the line emission

Although the fluxes from the wide slit data are all systematically higher than those from the narrow slit spectra, the poor seeing conditions in which the observations were made are expected to result in slit losses of $\sim 30\%$ for a point source, consistent with this difference. There is therefore no evidence for substantial extended emission to the north and south of the nucleus that would be encompassed by the wider slit only, although our uncertain flux calibration of the narrow slit data makes us rather insensitive to this. Regarding the possibility of emission being extended in an east–west direction, Table 1 indicates that increasing the size of the extraction aperture for the wide slit spectrum only produces a significant increase in the amount of [S III] λ0.9532 μm emission. This is also apparent by subtracting the 2-pixel spectrum from the 3-pixel one, which removes all the

emission lines except for [S III] and a marginal residual at the location of He I, although this might be the effect of the higher signal-to-noise ratio in these bright lines (see, for example, Simpson et al. 1996). We therefore find no significant differences between the morphologies of the different emission lines.

Our *IJ* echellogram (Figure 2) clearly shows the continuum peak drifting eastwards with decreasing wavelength. No such drift is seen in the locations of the emission line peaks and we can therefore rule out an incorrect order straightening algorithm as the cause of this effect. We measure an offset between the continuum and emission line peaks of $\lesssim 0\farcs5$ at Paβ, which increases to about $2''$ at the wavelength of [S III]. The magnitude and direction of this offset are consistent with the increasing contribution at short wavelengths of the infrared jet (Joy et al. 1986). At the longest wavelengths we observe, the continuum and line-emitting regions coincide, and therefore the line emission must come from the nucleus, since we know this is the origin of the K-band continuum emission.

3.3. Density of the emission region

Applying the extinction estimate derived above, the Hβ luminosity under Case B is $L_{\mathrm{H}\beta} = (8.0 \pm 1.0) \times 10^{31}$ W. This is larger than the Hβ luminosity in the nuclear disk of M 87 (Ford et al. 1994; assuming Hα/Hβ = 3.1), yet the emission in NGC 5128 comes from a much smaller region. This has implications for the density of the emission-line gas.

Emission line clouds of density n exposed to an ionizing photon flux ϕ will be ionized to a depth of $d \sim \phi/n^2\alpha_B$ (Ferland, Netzer & Shields 1979). Assuming that the clouds have $T = 10^4$ K and are located at a distance r from a compact radiation source which they surround with a covering factor $\Omega/4\pi$, the inferred Hβ luminosity requires a density

$$n \sim 4 \times 10^3 \left(\frac{U}{10^{-4}}\right)^{-1} \left(\frac{\Omega}{4\pi}\right)^{-1} \left(\frac{r}{10\,\mathrm{pc}}\right)^{2} \mathrm{cm}^{-3},$$

if the effective ionization parameter is U. We can rule out a picture where the emission-line clouds are embedded in an extended source of hard ionizing radiation (hard photons are needed to create a partially ionized zone which produces the [Fe II] emission) based on the observed rapid X-ray variability (Jourdain et al. 1993 and references therein).

For a planar shock with speed V covering an area d^2, and the scaling relation for Hβ luminosity of Dopita & Sutherland (1996), the preshock density needs to be

$$n \sim 1.1 \times 10^5 \left(\frac{V}{100\,\mathrm{km\,s^{-1}}}\right)^{-2.41} \left(\frac{d}{10\,\mathrm{pc}}\right)^{-2} \mathrm{cm}^{-3}.$$

We must consider these results when attempting to find a suitable model to explain the observed line emission.

3.4. Excitation mechanism

We observe a value of the reddening-insensitive ratio He I $\lambda 1.0830\,\mu$m/Pa$\gamma \approx 4$. This compares with typical values of ~ 2 (from Case B recombination and the observed He I $\lambda 0.4471\,\mu$m/Hβ ratio) in both H II regions (Doyon, Puxley & Joseph 1992) and AGN (Ferland & Osterbrock 1986), although larger ratios of 6.2 and 6.7 have been observed in Orion and NGC 4151, respectively (Osterbrock, Shaw & Veilleux 1990), and a ratio of 5.8 is predicted for the starburst galaxy NGC 3256 based on the observed He I $\lambda 2.06\,\mu$m/Brγ ratio (Doyon, Joseph & Wright 1994). We are therefore unable to discriminate between excitation scenarios, although this ratio does argue against arbitrarily high densities since collisional excitation readily increases the strength of the $1.0830\,\mu$m line.

Meadows & Allen (1992) suggest a starburst origin for the emission lines on the basis of their *HK* spectrum, and in particular the $H_2\,v$=1–0 S(1)/Brγ ratio. It should be noted that the dissociation temperature of H_2 is sufficiently low that the H_2 line emission cannot be produced cospatially with most of the other emission lines. This line ratio is therefore less than ideal for determining the excitation mechanism, and the observed ratio of 0.6 is equally consistent with both starburst and Seyfert galaxies (Moorwood & Oliva 1988). A starburst can, however, be excluded on the basis of the luminosity of the [Fe II] emission. Galactic supernova remnants typically have [Fe II] $\lambda 1.6435\,\mu$m luminosities of up to a few hundred $L_\odot$ (Oliva, Moorwood & Danziger 1989), although slightly higher (but far more uncertain) values have been determined for SNRs in external galaxies (van der Werf et al. 1993; Forbes et al. 1993). Adopting $L_{[\mathrm{FeII}]} = 10^3\,L_\odot$ for a single remnant, we require about 20 SNRs to power the observed emission (after correcting for extinction). Following the discussion of van der Werf et al. (1993), the radius of an individual SNR at the beginning of the radiative phase is $\sim 6\,$pc, and our spectroscopic observations indicate that the [Fe II] emission is at best barely resolved. Even making the generous assumption that the line-emitting region is spherical with a diameter of 20 pc, there is only room for at most 5 SNRs, and we can therefore rule them out as the excitation mechanism.

Of the observed emission lines, those of [Fe II] and [S III] have been the most well-studied, and we present a line ratio diagram in Figure 3. Few objects have been observed in both emission lines, and the plot is therefore sparsely populated. However, many more objects have been observed in one or other of the two emission lines, and it is seen that different classes of object are fairly well-separated in each of the separate ratios

(Simpson et al. 1996; Kirhakos & Phillips 1989). It is therefore possible to subdivide the parameter space as illustrated, and the objects do indeed lie in the expected regions. We also plot the theoretical line ratios as determined using the photoionization code CLOUDY V90.04 (Ferland 1996) for a plane-parallel slab with density $n_{\rm H} = 10^3$–$10^6\,{\rm cm}^{-3}$ illuminated by a power law spectrum extending from $10\,\mu$m to 50 keV with $\alpha = -1.4$ ($S_\nu \propto \nu^\alpha$), a range of ionization parameter $U = 10^{-2}$–10^{-5} and a gas phase iron abundance one-twentieth of solar. The high density model fits the data well, with $U \sim 10^{-4}$ explaining the observed LINER ratios, in line with studies using optical emission lines (e.g. Ferland & Netzer 1983). From this diagram, we are able to classify NGC 5128 as a LINER, although such objects are believed to differ from bona fide Seyfert galaxies only by virtue of possessing a less luminous active nucleus.

We have also detected the emission lines of [C I] $\lambda\lambda$0.9840,0.9850 μm and the [S II] λ1.0330 μm blend. These lines have also been detected in NGC 4151, with fluxes relative to [S III] λ0.9532 μm of 0.01 and 0.05 respectively (Osterbrock et al. 1990). We would expect stronger emission from these low-ionization lines in a less luminous source like a LINER, but there are no data from such sources to make comparisons with, and we must compare our data to the predictions of models. We again use CLOUDY for the photoionization models and MAPPINGS II (Sutherland & Dopita 1993) to investigate the effects of shock excitation, performing the same self-consistent iterative process described in Dopita & Sutherland (1996). Although the photoionization models were run with a low iron abundance to simulate depletion onto grains, the shock models used solar abundances, since grains would be destroyed by the shocks, liberating iron into the gas phase (Greenhouse et al. 1991).

Unfortunately, MAPPINGS II does not provide the strength of the He I λ1.0830 μm line in its output, and we are therefore unable to compare the observed value with its prediction. Instead, in Table 2, we present a lower value for the strength of this line, based on the Case B ratio of 4.41 times the strength of the He I λ0.4471 μm line.

Although we have not investigated all the parameter space for the shock models, due to the large computational effort involved, it is clear that shocks provide a rather better fit to the observed line ratios than do the photoionization models. In particular, photoionization fails to produce the observed line ratios over the range of ionization observed (C^0, S^+, S^{2+}), as has often been seen in the ultraviolet (e.g. Dopita et al. 1997). We therefore favor shocks as the dominant excitation mechanism, although ideally we would like some empirical evidence to support this conclusion, from observations of the same emission lines in other objects where the dominant excitation mechanism is known.

4. Discussion

The above arguments support the classification of NGC 5128 as a LINER, even though the emission lines which define this class (Heckman 1980) are not observable. This classification is not surprising, since it has also been applied to M 87 (Virgo A) on the basis of its optical emission line spectrum (Harms et al. 1994), and the similarities in the radio properties of NGC 5128 and M 87 are quite extensive (Tingay et al. 1998). Shock excitation was also favored over photoionization as the dominant process in M 87 (Dopita et al. 1997), and it is therefore not unexpected to find that the emission line gas in NGC 5128 lies in a disk (Schreier et al. 1998), just like in M 87 (Ford et al. 1994). We note, however, that we infer a lower shock speed, both in absolute terms and as a fraction of the Keplerian rotation speed at the radius we are observing.

The projected linear size of our narrow slit aperture is very similar to that of the 0.″26 FOS aperture used by Harms et al. (1994) to observe the nucleus of M 87, if we adopt their distance to M 87 of 15 Mpc. Harms et al. deduced the presence of a supermassive black hole in M 87 from variations in the line of sight velocity as a function of position near the nucleus, but they also observed that the emission lines were very broad (FWHM $\approx 1700\,\mathrm{km\,s^{-1}}$) at the location of the nucleus, due to the gravitational well of the black hole. Since the emission lines in NGC 5128 are unresolved at our resolution (FWHM $< 1000\,\mathrm{km\,s^{-1}}$), we infer that any supermassive black hole in NGC 5128 must be less massive than the $(2.4 \pm 0.7) \times 10^9\,M_\odot$ deduced for M 87 (Harms et al. 1994). If the velocity broadening is due to the rapid Keplerian rotation speed in the disk, then the black hole at the center of NGC 5128 can be no more than one-third as massive as that in M 87, i.e. $M_{\mathrm{BH}} \lesssim 10^9\,M_\odot$. Spectroscopy with higher spatial and spectral resolution would be valuable in further constraining the mass of the black hole.

Spectroscopic observations in the ultraviolet might also confirm our claim that the emission lines are powered by shocks, since the predictions of shock excitation and photoionization for lines such as C IV $\lambda 0.1550\,\mu$m and [Ne V] $\lambda 0.3426\,\mu$m can differ by factors of 10^4 (e.g. Dopita et al. 1997). Although there is significant extinction to the emission-line region, the emission lines are sufficiently bright (due largely to the proximity of NGC 5128) that these UV lines might still be detectable. Indeed, our shock model, coupled with $A_V = 3\,\mathrm{mag}$ of extinction, predicts $f_{\mathrm{C\,IV}} \approx 2 \times 10^{-18}\,\mathrm{W\,m^{-2}}$, which is detectable with the Space Telescope Imaging Spectrograph (STIS) on board the *Hubble Space Telescope*. However, we note that the C IV flux will be an order of magnitude fainter for every magnitude of visual extinction by which we have underestimated the true obscuration, and therefore its non-detection would not provide a definitive result.

5. Summary

We have presented near-infrared spectra of the nucleus of NGC 5128, covering the wavelength range 0.9–2.5 μm. The emission line ratios are characteristic of a LINER, and can be modeled fairly well by photoionization by a power law continuum or shock excitation, although shocks provide a noticeably better fit. For this reason, and on the basis of the similarities between Cen A and Vir A, we favor shocks as the dominant excitation mechanism in NGC 5128. Ultraviolet spectroscopy might be able to confirm this through the detection of high-ionization lines (e.g. C IV λ0.1550 μm), but the high obscuration in the UV could easily push them below a feasible detection threshold. We have inferred that the mass of a central black hole in NGC 5128 must be less than that in M 87 by a factor of at least 3.

We are grateful to Gary Ferland and the CLOUDY team for their dedication to the development and support of CLOUDY. This work was performed at the Jet Propulsion Laboratory, California Institute of Technology, under a contract with the National Aeronautics and Space Adminstration. VM was supported for these observations by an Australian Postgraduate Research Award. We thank the Anglo-Australian Observatory for generous access to its computing and other facilities. We also wish to thank David Allen for assistance in acquiring the spectra and for many useful discussions.

REFERENCES

Allen, D., et al. 1993, Proc. ASA, 10, 298

Baade, W., & Minkowski, R. 1954, ApJ, 119, 215

Cardelli, J. A., Clayton, G. C., & Mathis, J. S. 1989, ApJ, 345, 245

Clarke, D. A., Burns, J. O., & Norman, M. L. 1992, ApJ, 395, 444

De Koff, S., et al. 1996, ApJS, 107, 621

Dennefeld, M. 1986, A&A, 157, 267

Dopita, M. A., & Sutherland, R. S. 1996, ApJS, 102, 161

Dopita, M. A., Koratkar, A. P., Allen, M. G., Tsvetanov, Z. I., Ford, H. C., Bicknell, G. V., & Sutherland, R. S. 1997, ApJ, 490, 202

Doyon, R., Puxley, P. J., & Joseph, R. D. 1992, ApJ, 397, 117

Doyon, R., Joseph, R. D., & Wright, G. S. 1994, ApJ, 421, 101

Ferland, G. J. 1996, *Hazy, a brief introduction to Cloudy*, University of Kentucky Department of Physics and Astronomy Internal Report.

Ferland, G. J., & Netzer, H. 1983, ApJ, 264, 105

Ferland, G. J., & Osterbrock, D. E. 1986, ApJ, 300, 658

Ferland, G. J., Netzer, H., & Shields, G. A. 1979, ApJ, 232, 382

Forbes, D. A., Ward, M. J., Rotaciuc, V., Blietz, M., Genzel, R., Drapatz, S., van der Werf, P. P., & Krabbe, A. 1993, ApJ, 406, L11

Ford, H. C., et al. 1994, ApJ, 435, L27

Giles, A. B. 1986, MNRAS, 218, 615

Greenhouse, M. A., Woodward, C. E., Thronson, H. A., Rudy, R. J., Rossano, G. S., Erwin, P., & Puetter, R. C. 1991, ApJ, 383, 164

Harms, R. J., et al. 1994, ApJ, 435, L35

Heckman, T. M. 1980, A&A, 87, 152

Jackson, N., & Eracleous, M. 1995, MNRAS, 276, 1049

Jourdain, E., et al. 1993, ApJ, 412, 586

Joy, M., Harvery, P. M., Tollestrup, E. V., Sellgren, K., McGregor, P. J., & Hyland, A. R. 1991, ApJ, 366, 82

Kirhakos, S., & Phillips, M. M. 1989, PASP, 101, 949

Meadows, V., & Allen, D. 1992, Proc. ASA, 10, 104

Meier, D. L., et al. 1989, AJ, 98, 27

Moorwood, A. F. M., & Oliva, E. 1988, A&A, 203, 278

Nussbaumer, H., & Storey, P. J. 1988, A&A, 193, 327

Oliva, E., Moorwood, A. F. M., & Danzjiger, I. J. 1989, A&A, 214, 307

Osterbrock, D. E. 1983, PASP, 95, 12

Osterbrock, D. E., Shaw, R. A., & Veilleux, S. 1990, ApJ, 352, 561

Quillen, A. C., Graham, J. R., Frogel, J. A. 1993, ApJ, 412, 550

Schreier, E. J., et al. 1979, ApJ, 234, L39

Schreier, E. J., et al. 1998, ApJ, 499, L143

Simpson, C., Forbes, D. A., Baker, A. C., & Ward, M. J. 1996, MNRAS, 263, 777

Soria, R., et al. 1996, ApJ, 465, 79

Thomson, R. C. 1992, MNRAS, 257, 689

Tingay, S. J., et al. 1998, AJ, 115, 960

Turner, P. C., Forrest, W. J., Pipher, J. L., & Shure, M. A. 1992, ApJ, 393, 648

van der Werf, P. P., Genzel, R., Krabbe, A., Blietz, M., Lutz, D., Drapatz, S., Ward, M. J., & Forbes, D. A. 1993, ApJ, 405, 522

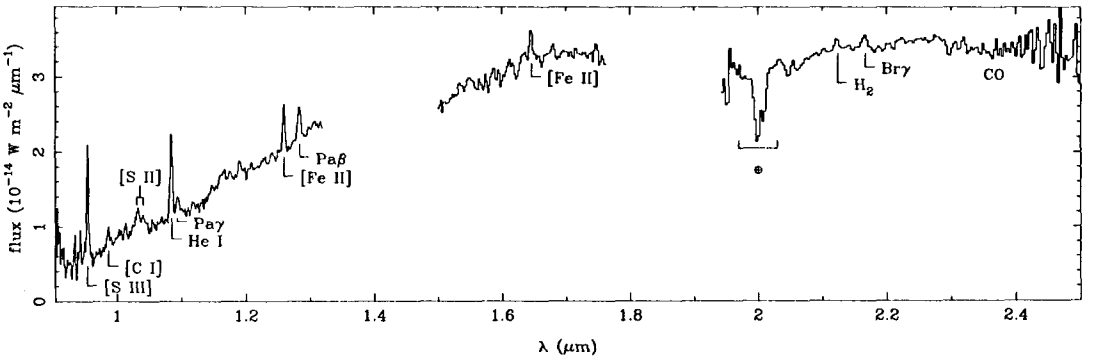

Fig. 1.— Nuclear spectrum of NGC 5128, extracted through a 1.″4 × 1.″6 aperture. The emission lines are labeled, as are regions of CO and atmospheric absorption. This spectrum was taken in non-photometric conditions, and the flux scale has been bootstrapped as described in the text.

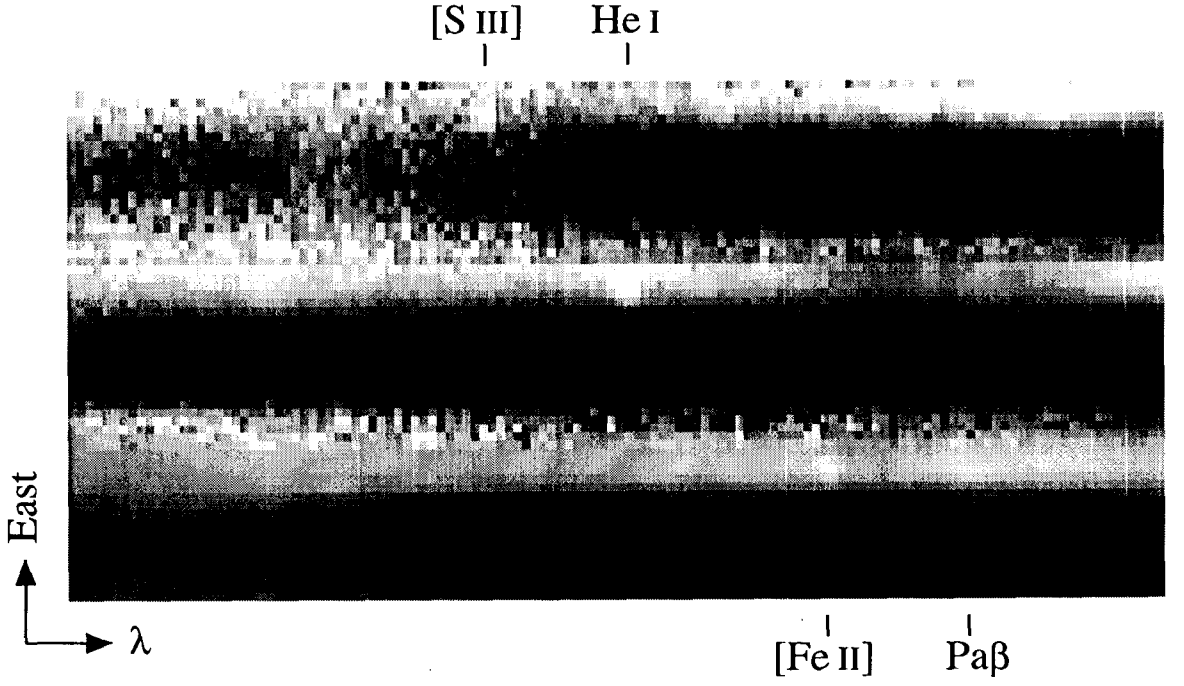

Fig. 2.— Part of the narrow slit *IJ* echellogram. Within each order, the wavelength and spatial directions are as indicated. The topmost order covers the shortest wavelengths. The locations of the most prominent emission lines are indicated. Note how at short wavlengths the continuum is displaced eastwards from the line emission.

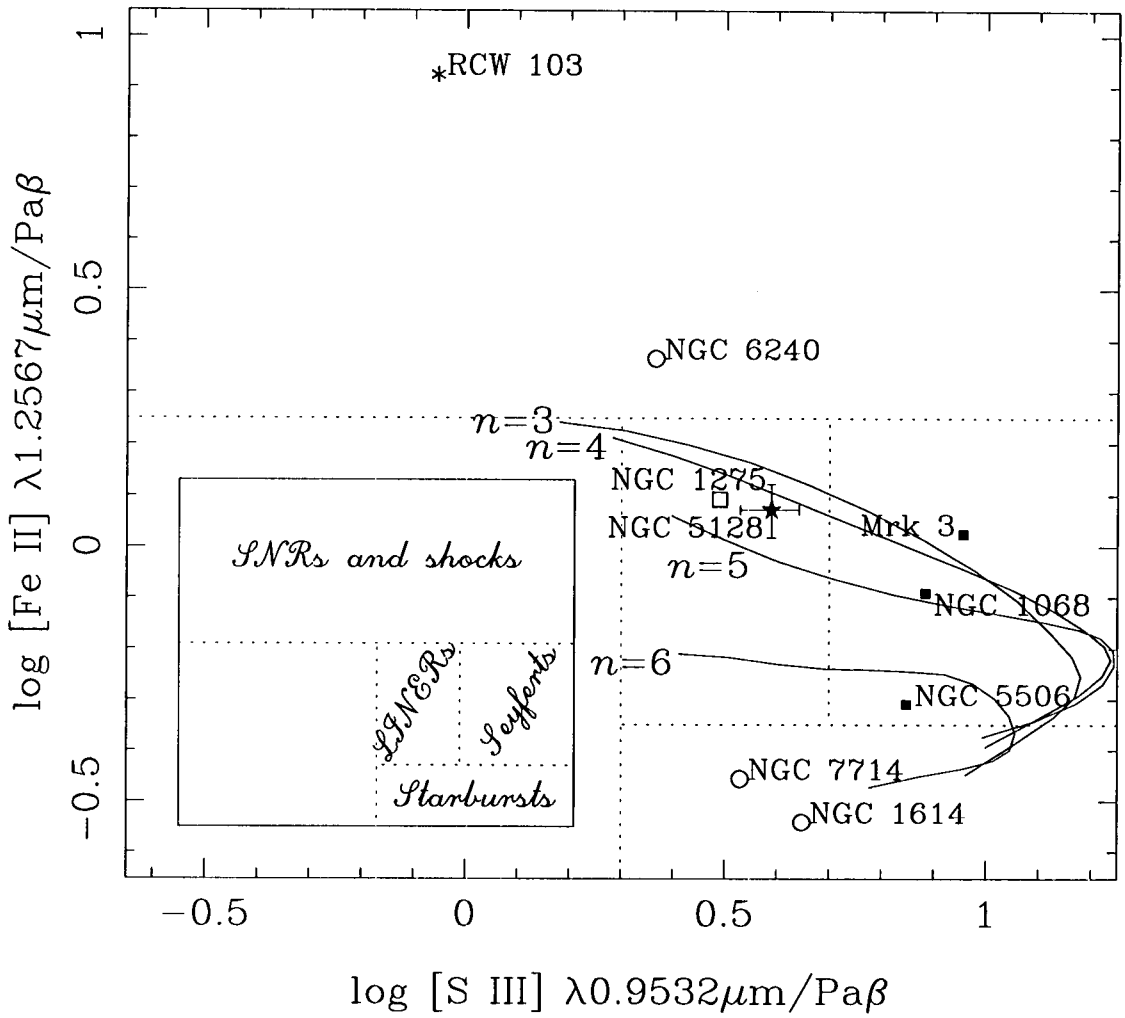

Fig. 3.— [Fe II]/Paβ *vs* [S III]/Paβ line ratio diagram. The regions expected to be occupied by different classes of object are separated by dotted lines as shown in the inset, and those few objects for which data exist for both forbidden lines are plotted. We have plotted reddening-corrected line ratios for Seyfert galaxies (solid squares), starburst galaxies (open circles), and the LINER NGC 1275 (open square), using data from Kirhakos & Phillips (1989) and Simpson et al. (1996 and references therein), assuming Case B ratios to convert Hα and Brγ fluxes to Paβ. The six-pointed star is the Galactic supernova remnant RCW 103 (Dennefeld 1986). The solid lines are theoretical photoionization models of different densities, as described in the text.

Table 1: Emission line fluxes through the different spectroscopic apertures. The 1.″4 × 1.″6 aperture measurement have been calibrated as described in the text, and are subject to a ∼ 20% systematic uncertainty, in addition to the random errors listed. Fluxes indicated with a dagger (†) are strongly affected by an uncertain background level as a result of poor OH line subtraction.

	$\lambda_{\rm rest}$	Line fluxes (10^{-18} W m^{-2})		
Line	(μm)	1.″4 × 1.″6	5.″8 × 1.″6	5.″8 × 2.″4
[S III]	0.9532	54 ± 4	75 ± 7	100 ± 10
[C I]	0.9850	10 ± 1	17 ± 2	17 ± 3
[S II]	1.0330	40 ± 5	95 ± 9	120 ± 15
He I	1.0830	50 ± 4	110 ± 20†	150 ± 30†
Paγ	1.0939	12 ± 2	33 ± 8†	48 ± 12†
[Fe II]	1.2567	26 ± 2	33 ± 3	32 ± 5
Paβ	1.2819	22 ± 2	35 ± 5	40 ± 4
[Fe II]	1.6435	25 ± 4	80 ± 20†	79 ± 13†
H_2 v=1–0 S(1)	2.1213	11 ± 2	17 ± 2	27 ± 5
Brγ	2.1657	17 ± 3	28 ± 4	— †

Table 2: Comparison of excitation models. All fluxes have been normalized to Paβ = 100, and the observations have been corrected for reddening. The photoionization model has $n_{\rm H} = 10^5\,{\rm cm}^{-3}$ and $U = 10^{-4}$. The shock excitation model is for a 120 km s^{-1} shock with precursor in a medium with density $n_{\rm H} = 3 \times 10^4\,{\rm cm}^{-3}$ and an equipartition magnetic field.

Line	$\lambda_{\rm rest}$ (μm)	Measured	photo	shock
[S III]	0.9532	393 ± 29	849	390
[C I]	0.9850	68 ± 7	62	50
[S II]	1.0330	251 ± 31	682	186
He I	1.0830	291 ± 23	1291	> 109
[Fe II]	1.2567	121 ± 9	77	94
Paβ	1.2819	100 ± 9	100	100